



Mechanical and Fatigue Damage Evolution Properties of Cracked Sandstone under Cyclic Loading

Yuan Xu, Fengyu Ren, Zulkifl Ahmed*, and Kaiyi Wang

School of Resource and Civil Engineering, Northeastern University, Shenyang 110819, China

Abstract: To analyze the mechanical parameters and fatigue damage evolution under uniaxial compression, the stress strain curve, failure process characteristics, strength properties and deformation of cracked sandstone specimens were studied under various stress conditions. Initially, during loading and unloading periods, the optical images of sample were presented for digital image correlation (DIC) analysis. After this, sandstone samples subjected to cyclic loading with different crack parameters were tested with electric universal machine. Within the framework of origin software, the damage variable of cracked sandstone samples was defined by the strain variation analysis. The results exhibited that the dissimilarity of mechanical parameters under cyclic loading was closely associated to the experimental situations. The elastic modulus (E) of the samples under cyclic loading showed a “strengthening” phenomenon. With the increase of crack bridge inclination angle (β), the peak strength decreased firstly and then increased regularly. While, with the increase of crack inclination angle (α), the crack initiation stress and peak strength increased first and then decreased linearly. By using the fitting analysis of the damage evolution equation, it was proved that the damage variable definition method was suitable for the damage-evolution characteristics of prefabricated cracked sandstone.

Keywords: Fatigue damage, Elastic modulus, Pre-fabricated cracked sandstone, Cyclic load, Failure mode, Mesoscopic mechanism, Damage variable.

1. INTRODUCTION

Due to the development and constant movement of the crust, there are certainly a huge number of defects such as cracks, joints and micro pores in the rocks. With the development and propagation of cracks, the damage and deformation of a rock is strongly restricted and affected by internal and external flaws, particularly structural planes with joints scale [1]. So, research on the characteristics and fatigue damage evolution progress of rock-mass under the condition of uniaxial or tri-axial compression is of great importance to tunnel engineering, mining engineering, and geotechnical engineering. Large attentions have been made during the past few decades to understand the impact of cyclic loading on the rock-masses. It was informed that the fatigue parameters of rock were dependent on the frequency, maximum stress, loading, amplitude and waveform [2-5]. It is also documented previously that the loading conditions significantly influence the fatigue properties of

rock-masses. The uniaxial and tri-axial compressive strength decreases with the increase in the number of cycles and the applied stress level [6]. Tien et al.(1990) [7] developed a relationship between the fatigue life and the accumulation of axial strain of the sandstone based on the findings from the cyclic loading’s tests. Furthermore, to measure the influence of frequency on the strength properties of sandstone specimens subjected to cycling loading a series of laboratory tests were conducted in the confining stress state [8]. On the other hand, some theoretical work has also been conducted on the fatigue of rocks such as the relationship between strength and energy dissipation, global failure and energy release during the failure and deformation of rocks [9]. Xiao et al. (2009) [10] presented an inverted S-shaped nonlinear fatigue damage cumulative model based on the law of axial irreversible deformation development of rock.

Damage is a phenomenon whereby micro defects in a material under monotonic loading

or reloading leads to a progressive decrease in the cohesion and damage of volume units. Many scholars at home and abroad have carried out systematic research into the damage evolution characteristics and constitutive models of rock, and have achieved some remarkable results in this field. Yun-De et al. (2004) [11] studied the complete stress–strain curve characteristics of marble under triaxial compression, and established the bilinear elastic-linear strain-softening residual ideal plastic damage constitutive model. Ren. (2010) [12] studied the damage evolution laws of coal and the rock-mass using a computerized tomography triaxial loading system, realizing the quantitative evaluation of the damage state. Jin et al.(2013) [13] studied damage evolution of rock under uniaxial compression and built the coal-rock damage evolution model which considered residual strength based on electromagnetic radiation characteristics. Zhang et al. (2011) [14] studied the deformation and failure mechanism of strong weathered sandstone by tri-axial compression testing, and analyzed the damage evolution processes and established damage evolution equations based on the density method. Ni et al.(2012) studied the microscopic damage characteristics of siltstone under tri-axial compression by scanning electron microscopy and digital image technology, and analyzed the statistical distribution characteristics of azimuth angle, length and width of cracks [15] . Damage of marble induced by cyclic loading was recorded through interferometric technique [16]. Zhou et al. (2010) [17] studied the strength, deformation and fracture damage characteristics of sandstone by uniaxial cyclic loading and unloading tests, and defined a damage variable based on linear damage mechanics theory and acoustic emission (AE). Wen et al.(2014) [18] established a new damage model and a statistical damage constitutive model of rock under specific confining pressure according to the force of the damaged and undamaged parts in rock on the base of statistical damage theory. Jiang et al. (2009) [19] studied the damage evolution characteristics in the whole uniaxial compression process of sandstone by electrical resistivity and AE, and proposed a status qualitative criterion for rock damage. The indicators such as AE, density, electrical resistivity and crack length were adopted to evaluate the degree of damage and to study the damage evolution laws of rock in related research. However, research on the damage evolution process

of pre-fabricated cracked sandstone on the basis of the strength properties (elastic modulus) is less well developed.

Digital image correlation (DIC) is an effective method, among kinds of experimental methods, for determining strain fields and displacement on the surface of specimen which could be of real-time, full-field, online, flexibility and non-contact [20, 21]. Under different loadings condition this method had been successfully applied to observe the deformation of rock [22, 23]. Moreover, crack propagation and deformation evolution of rock under cyclic indentation were described using the apparent strain field obtained by DIC Zhang et al. (2013) [24].

Hence, in this research, the failure process, evolution laws, mechanical properties and deformation modes of prefabricated cracked sandstone under different crack parameters (α and β) studied by uniaxial compression tests and digital image correlation (DIC) method.

2. EXPERIMENTAL SETUP AND METHODOLOGY

2.1 Experimental System and Specimens

The experimental setup for compression testing involves electric universal machine, a computer for capturing and processing the images and a high pixel's camera (Fig. 1). The schematic and physical drawings of the test device are shown in Fig. 1. The sandstone specimens were collected from Junan County, Linyi City, Shandong Province, China. The dimension of sample was $25 \times 25 \times 50$ mm (Fig. 2). The crack geometric parameters were crack dip angle α , bridge dip angle β , crack length l , and bridge length w (Fig. 2). The basic physical



Fig. 1. Rock specimen and experimental apparatus

parameters of the cracked sandstone samples are summarized in Table 1.

The length (l) and width (t) of the pre-fabricated upper and lower cracks were 10 mm and is 2 mm, respectively. The length of the rock bridge was $w = 15$ mm. The crack inclination angle was α and the rock bridge inclination angle was β as shown in Fig. 2. In order to obtain the failure mode with different crack parameters (α , β , l and w), two different M and N groups of specimens were designed (Table 2). M and N group is divided into five subgroups as shown in Table 2. The uniaxial compression test was carried out on the group M1 and N1, and the uniaxial cyclic loading and unloading tests were carried out on the group M2 and N2. In this way, the effects of loading mode on the mechanical properties of intact sandstone and cracked sandstone were explored in this study. The uniaxial cyclic loading and unloading tests were carried out on the samples of the M3-M5 and N3-N5 group to explore the variation law of the mechanical properties of the samples under different rock bridge

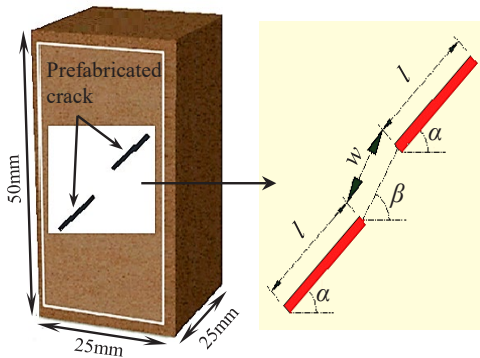


Fig. 2. Dimension of specimens and geometric parameters of pre-fabricated cracks

Table 1. Basic physical parameters of sandstone samples

W/mm	L/mm	H/mm	$\rho/(kg/m^3)$	E/GPa	R_c/MPa
25	25	50	2411	9.63	56.12

Note: W -width; L -Length; H -Height

Table 2. Crack geometry parameters of sandstone samples (M and N groups) samples

Group	$\alpha/^\circ$	$\beta/^\circ$	Group	$\alpha/^\circ$	$\beta/^\circ$
M1	45	30	N1	30	75
M2	45	45	N2	45	75
M3	45	60	N3	60	75
M4	45	75	N4	75	75
M5	45	90	N5	90	75

inclination and crack inclination. Digital image correlation (DIC) method and origin software were used to observe the failure of sandstone samples.

2.2 Principle of Digital Image Correlation Method

In the field of experimental mechanics DIC is considered as an optical measurement method which has been extensively used for deformation measurement [25, 26]. The basic principle of DIC is to track the same pixel points based on the comparison of an undeformed image with a deformed image. As illustrated in Fig. 2, a square subset is chosen to compute the displacement of one point which was centered at the point in the undeformed image. The matching process is completed through searching the maximum correlation coefficient between the target subset and reference subset. Then the displacement fields of analysis region were determined by adopting the method presented by Mudassar et al. (2016) [26]. The displacement measurement accuracy in present test was at least $1 \mu m$. Point wise least squares method is also used to determine apparent strain fields [27].

2.3 Loading Procedure and Data Acquisition

Two dial gauges were placed symmetrically in the middle of the sample to characterize the lateral deformation characteristics of the sample during the cyclic loading. The loading and unloading rates were 300N/s. Loading was applied with a speed of 0.15 mm/min. The loading and unloading test schemes were as follows: each specimen is subjected to six-week loading and unloading cycle. The cyclic upper limit stress levels of the intact sandstone were 24.0, 26.0, 28.0, 30.0, 32.0 and 34.0 MPa. Rock samples are constantly loaded until it deforms.

2.4 Definition of Fatigue Damage Variable

Damage is a formation progress of micro-cracks or micro-voids in a rock block. Damage leads to the change of materials properties, e.g., the hardness, elastic modulus, density, residual strain and residual [28]. Consequently, the approaches to define damage are numerous and the ones often used consist of elastic modulus, maximum strain, energy

dissipation, residual strain, acoustic emission (AE) and ultrasonic wave velocity methods [28]. No matter what kind of parameter is used, the damage evolution must be consistent with the stable, unstable and initiation, propagation of microcracks [29]. Therefore, a realistic damage variable must encounter the fundamental needs: it has diverse physical meaning; it can be applied in engineering handily and measured easily; its evolution law matches well with the real ruin process of rock-masses.

2.4.1 Elastic modulus method

Damage variable (D) can be expressed as the loss of stiffness as:

$$D = 1 - \frac{E}{E_0}$$

where E represents the actual modulus and E₀ represents the Young's modulus of damaged and undamaged sandstone samples respectively.

The deterioration of elastic modulus of both M and N group of sandstone samples is shown in Fig. 3. As the number of cycles increases the elastic modulus (E) decrease for both samples (Fig. 3). There is no difference between the both specimens (M and N) in fatigue damage evolution. It seems problematic to acquire the preliminary elastic modulus. Moreover, in this method the fatigue preliminary damage is not taken into account. So, even though the elastic modulus technique is used expansively for its discrete physical meaning, it is found unsuitable for describing the whole fatigue damage process of rock.

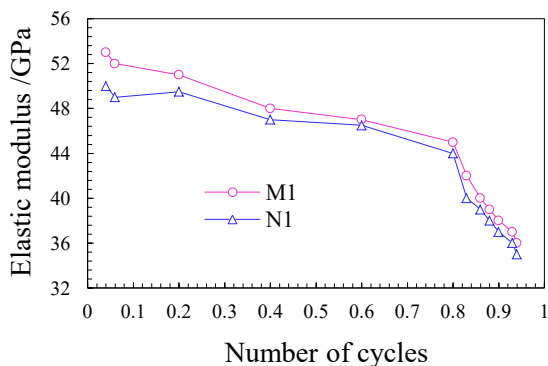


Fig. 3. Decay curve of elastic modulus

2.4.2 Maximum strain method

Damage variable can be defined with maximum strain as:

$$D = \frac{\varepsilon_{max}^n - \varepsilon_{max}^0}{\varepsilon_{max}^f - \varepsilon_{max}^0}$$

where ε_{max}^0 , ε_{max}^n and ε_{max}^f are the initial maximum strain, instantaneous maximum strain after n cycles and ultimate maximum strain, respectively. The damage evolution curve of specimen M and N group can be seen in Fig. 4. While the maximum strain method is utilized to define damage of sandstone. Damage increases as the number of cycle increases (Fig. 4). Apparently, the maximum strain technique leaves the fatigue out of thought and magnifies the damage formed by cyclic loading. Thus, this method seems unsuitable for quantifying the fatigue damage process based on the fact that, generally speaking, the initial damage of rock is great due to past complex load history.

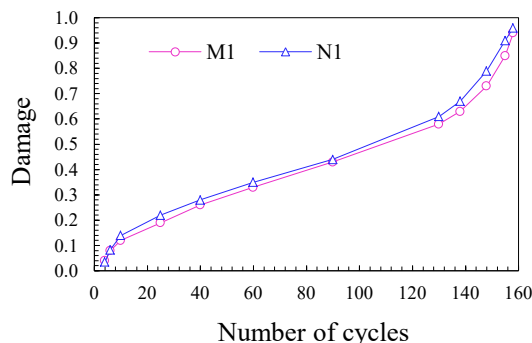


Fig. 4. Damage evolution curve of specimens M1 and N1

3. EXPERIMENTAL RESULTS AND ANALYSIS

3.1 Effect of Loading Mode on Mechanical Properties of Sandstone

The mechanical properties (elastic modulus and peak strength), in this study, is determined by the slope of approximate linear section of stress-strain curve with the help of origin software. The effect of loading on the elastic modulus and peak strength of M and N group of sandstone is presented in Table 3. The cyclic loading has a “strengthening” effect on the elastic modulus on the mechanical properties of cracked sandstone as can be observed in Table 3. Under the cyclic loading, the increase range in peak strength of the cracked sandstone samples is 14.7%.

After six weeks of loading and unloading cycles, the elastic modulus of the sample is greatly improved compared with the elastic modulus measured by the laboratory test. In order to understand the effects of loading mode on the peak strength of sandstone samples more comprehensively, the authors have collected the results of Zhou et al. (2010) [17] study and compare with current results and the following rules are found in Table 3.

The uniaxial cyclic unloading and loading action may weaken the peak strength of prefabricated cracked sandstone samples or increase its peak strength. When the peak strength of the specimens under cyclic unloading and loading was higher than its uniaxial compressive strength was lower. Higher the compactness and uniaxial compressive strength of the specimen, more likely the “weakening” phenomenon occurred under cyclic loading. The cyclic loading can weaken the peak strength of both intact samples and cracked samples with macroscopic defects. The effect of cyclic loading on the elastic modulus of the sandstone samples is closely related to cyclic stress path and its lithology. When similar cyclic unloading and loading paths were applied to samples with different lithology, the mechanical effects are quite different. The mechanical response of specimens under cyclic unloading and loading is closely associated to its stress condition. The “strengthening” phenomenon of elastic modulus is more likely to occur during cyclic loading.

3.2 Meso-Mechanism Analysis of Elastic Modulus

In current research origin computer code is selected for meso-mechanism analysis in the variation of elastic modulus. Fig. 5 shows the change in elastic modulus of sandstone samples under different crack geometric parameters. It can be clearly observed from Fig. 5(a) that the elastic modulus of

samples M1, M2 and M4 suddenly increased, but the elastic modulus of M3 and M5 first increased then decreased as the number of cycles increased. The elastic modulus of samples N1, N3 and N5 gradually increased, but the elastic modulus of sandstone samples N2 and N4 first increased then decreased as the number of cycles increased. For different cyclic loading modes, the elastic modulus after six-weeks of loading was increased significantly compared with the elastic modulus measured by uniaxial compression tests.

In the natural state, there are a large number of primary defects in the pre-fabricated cracked sandstone samples. At the first loading phase, a large number of primary micro-cracks inside the sample were compacted, and in the unloading stage, only a few micro-cracks were recovered in this work. Therefore, the compactness of sample is improved greatly after the first week of loading and unloading phases. However, it is noteworthy that the “strengthening” phenomenon of elastic modulus does not occur in all specimens. But some specimens show the “weakening” phenomenon of elastic modulus during cyclic loading and unloading, especially in M1 group. The “weakening” phenomenon of these specimens with prefabricated cracks is closely related to the development of macro-cracks during cyclic loading and unloading.

3.3 Analysis of Stress-Strain Curve for Cracked Samples

The stress–strain curves of sandstone samples after different loading cycles are shown in Fig. 6. Most significant degradation of elastic modulus occurring in N1 sample as figures shows. It can be seen from Fig. 6(a) that the loading and unloading cyclic curve of each stage is concave, and the loading and unloading paths of the curves coincide with each other, which leads to the formation of plastic

Table 3. Variation of mechanical parameters of specimens under different loading modes

Specimen	Peak strength/MPa	Elastic modulus/GPa	Specimen	Peak strength/MPa	Elastic modulus/GPa
M1	49.3	8.58	N1	68.3	9.35
M2	56.4	9.23	N2	58.8	8.97
M3	55.3	8.68	N3	57.9	8.89
M4	34.6	7.07	N4	53.1	9.46
M5	41.2	8.87	N5	45.2	9.73

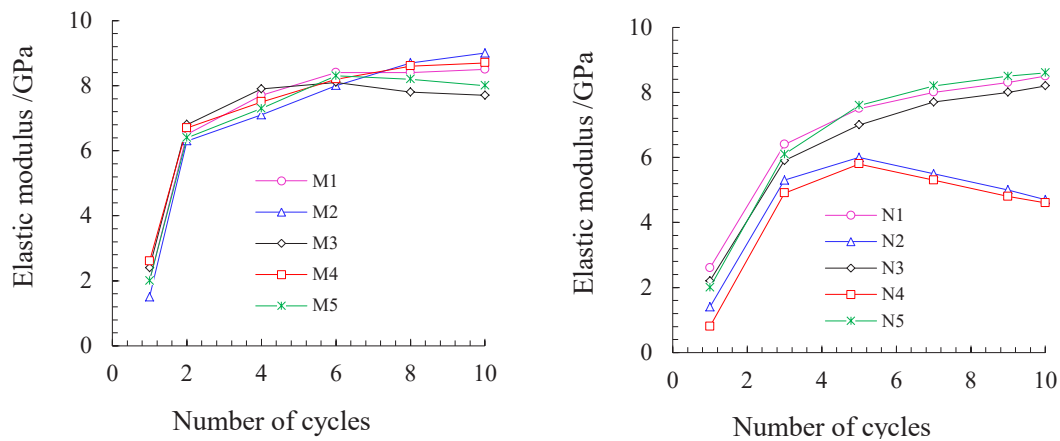


Fig. 5. The effect of fracture geometric parameters on the variation of elastic modulus, (a) variation of elastic modulus of M group and (b) variation of elastic modulus of N group.

hysteresis loops. With the increase of cycle number, in case of N group of samples, the hysteresis loops move towards the direction of strain increase as shown in Fig. 6(b). The irreversible deformation of the specimen increases ceaselessly.

3.4 Effect of Crack Geometric Parameters on Stress Eigenvalues

This sub-section mainly discusses the effect of crack geometric parameters (α and β) on the peak strength and crack initiation stress of sandstone samples. Origin software is selected in current study to develop relationship between crack geometric parameters i.e., α and β and stress eigen values (Fig. 7). For the convenience of the

following description, the peak stress and the crack initiation stress are collectively referred to as “stress eigenvalues”. The effect of fracture geometric parameters on the stress eigenvalues of specimens is shown in Fig. 7. It can be seen from Fig. 7(a) that as the increase of α from 20° to 90° , the average peak strength increased from 21 MPa to 46 MPa. The average crack initiation stress increased from 19 MPa to 33 MPa. It can be seen from Fig. 5(b) that when β increased from 20° to 75° , the average peak strength decreased from 39 MPa to 28 MPa. The average crack initiation stress decreased from 30 MPa to 19 MPa. This phenomenon reflects that the crack inclination angle in the range of 75° to 90° has little effect on the stress eigenvalues of sandstone samples. Compared with Fig. 7(a) and

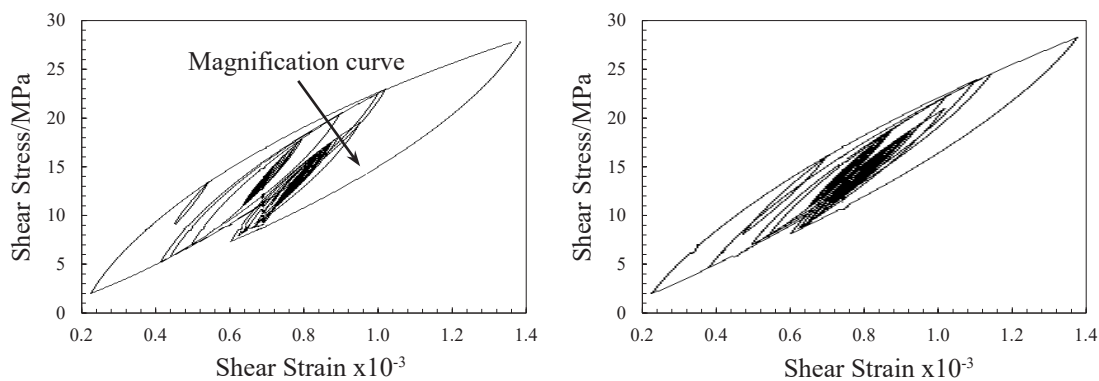


Fig. 6. Stress-strain curves of sandstone specimens after first six weeks of loading and unloading cycle, (a) specimen M1 and (b) specimen N1

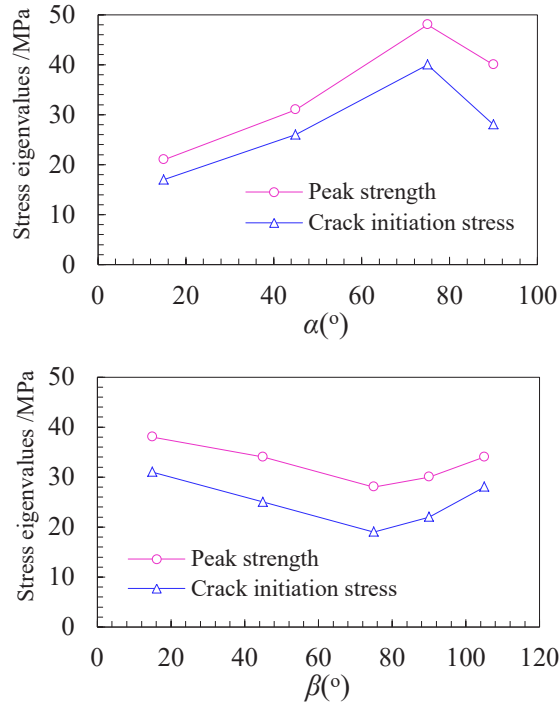


Fig. 7. Effect of fracture geometric parameters on stress eigenvalues, (a) Effect of crack inclination on stress eigenvalues and (b) Effect of rock bridge inclination on stress eigenvalues

Fig. 7(b), it is not difficult to find out that the effect of crack inclination on stress eigenvalues of cracked sandstone are more significant. The variations of crack initiation stress and peak strength with the crack geometric parameters are not similar.

3.5 Effect of Rock Bridge Inclination on the Failure Mode of Sandstone

Figure 8 shows the failure pattern of pre-fabricated cracked sandstone specimens with different inclination angles of β . The order of capitals in the diagram indicates the sequence of crack initiation at the same time. As shown in Fig. 8(a), when $\beta = 30^\circ$, the sample first produced a tensile crack “A”. As the axial stresses increased, the crack “A” gradually developed along the direction of the maximum principal stresses. Then a new tensile crack “C” was initiated near the pre-fabricated crack as shown in Fig. 8(a). Along with the instability failure of the sample, the shear crack “B” was initiated in the middle of the pre-fabricated crack and quickly merged with the crack C, and finally propagate downward to the lower end of the sample and form

a new big tensile crack “D” (Fig. 6a).

When $\beta = 45^\circ$, two secondary oblique crack A and C initiated near the pre-fabricated crack and the bottom of the sample, respectively, (Fig. 8b). Also, a shear wing crack initiated from “B” as shown in Fig. 8(b).

Subsequently, a big tensile crack initiated from the top of sample and passes from bottom of sample (Fig. 8b). As shown in Fig. 8(c), when $\beta = 60^\circ$, the sample firstly generated a secondary coplanar crack “A” from the right upper corner of sample and then three wing crack B, C and D produced approximately perpendicular with pre-fabricated crack. The areas of rock-bridge had a tensile and shear composite coalescence (Fig. 8c). As the axial stresses continue to increase, the crack a propagated toward the maximum principal stress, and eventually developed to the upper end of the specimen.

When $\beta = 75^\circ$ as shown in Fig. 8(d), three tensile cracks B, D and I were first initiated from the upper and lower end of sample. Then two shear wing cracks A and C were initiated near the crack “B” and form 90° angle with each other (Fig. 8d). Also, two secondary crack F and H initiated near the pre-fabricated crack as shown in Fig. 8(d). Finally, two shear wing cracks produced from pre-fabricated crack and emerge with main tensile crack D, (Fig. 8d), which leads to the phenomenon of tensile coalescence in the rock bridge area. When $\beta = 90^\circ$, as shown in Fig. 8(e), the wing crack “D” was first produced, and then five new wing cracks A, B, C, E and I was initiated from the upper and middle part of the sample. As the axial deformation increased, the crack F was initiated from crack D and then emerged with E (Fig. 8e). Subsequently, the tensile crack G was initiated at the lower end of sample. At the same time, the crack D expanded significantly along the direction of the maximum principal stress. With the failure of the sample, the crack F overlapped and merged with the crack E of the sample.

Observing the failure mode of different crack bridge angle, under this experimental condition, it is found that the crack initiation phenomenon occurs at the tip of the prefabricated crack mostly. This is due to the existence of pre-fabricated crack and

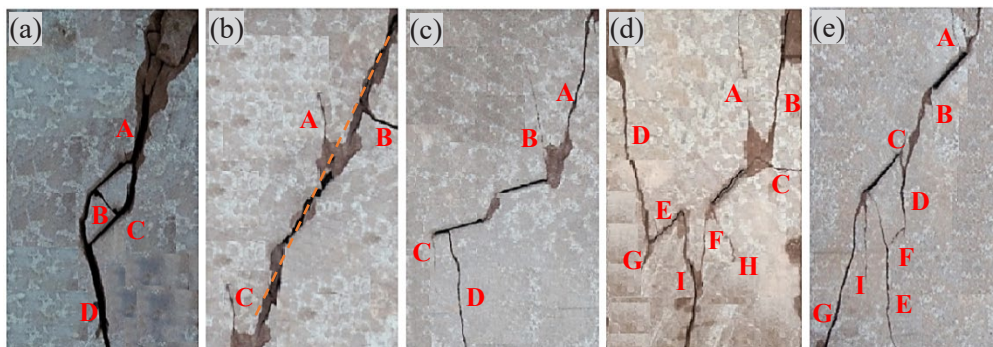


Fig. 8. Fracture model diagram of samples with different rock bridge angles (a) $\beta = 30^\circ$ (b) $\beta = 45^\circ$ (c) $\beta = 60^\circ$ (d) $\beta = 75^\circ$ (e) $\beta = 90^\circ$

stress concentration at the crack tip. The inclination parameters of Rock Bridge have great effect on crack propagation and rock bridge coalescence mode. When β was 75° , the rock bridge area usually does not fail (Fig. 8e). When β was 30° , 45° and 90° , the rock bridge area has a tensile coalescence.

3.6 Effect of Crack Geometric Parameters on Failure Type

This sub-section investigates the effect of crack geometric parameters on the value of tensile crack ratio. It can be seen from Fig. 9 that as the crack inclination angle “ α ” and bridge inclination angle “ β ” increased, the tensile crack ratio of the samples first suddenly decreased and then tends to be unchanged.

It is reflected that under the conditions of this test, when the crack inclination angle is in the range of 40° , the effect on the type of failure of the sample was more. According to the statistics of crack types and number of all specimens observed in this test, tensile crack accounts for 67.9%, shear crack accounts for 26.3%, and the main failure mode of

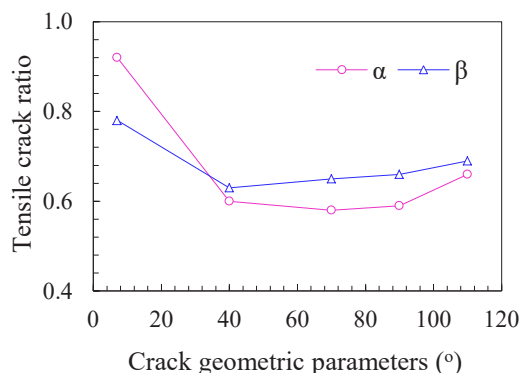


Fig. 9. Effect of fracture geometric parameters on the value of tensile crack ratio^o

the specimen is tensile failure.

3.7 Relationship Between Micro Damage and Peak Strength Degradation

Peak strength of the sandstone can be quantified by a strength degradation parameter (S), which can be defined as:

$$S = \frac{\sigma_i - \sigma_d}{\sigma_i}$$

where σ_i represents the original peak strength and σ_d represents the peak strength of intact and damaged sandstone samples respectively.

After cyclic loading, the samples are tested under compression until completely deformed. The stress–strain curves of sandstone samples at different pre-fabricated crack inclination angle are generated with origin software (Fig. 10). Under cyclic loading, the stresses are continuously redistributed in the samples and the fracture toughness decreases allowing more subcritical crack to grow which consequently leads to stress corrosion and mechanical properties degradation.

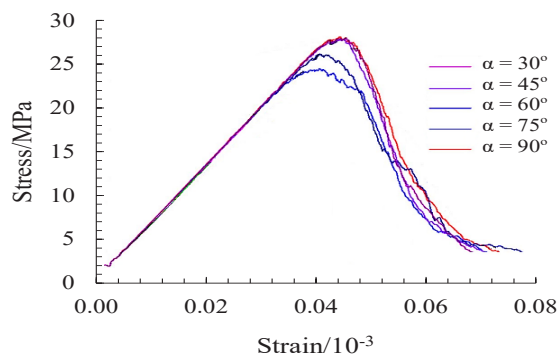


Fig. 10. Stress-strain curve diagram of samples at various prefabricated crack angles

Moreover, the prefabricated crack weakens the structure and cementing capability of the sandstone samples, therefore micro flaws or cracks would propagate and grow quickly under cyclic load [17]. It can be seen from the description of above subsections that the most samples mainly appear the “strengthening” phenomenon of modulus of elasticity under cyclic load, but a few numbers of samples have weakened the elastic modulus. Fig. 11(a-c) shows the crack propagation of the sample M1 after the end of the second, third and fourth cycles, respectively. Fig. 11(d) shows the crack propagation at the time of final failure of the specimen. Fig. 11 also shows the failure diagram of samples after different cyclic load. During the second loading process, the macroscopic cracks were not observed on the surface of the sample, and the “strengthening” trend remained (Fig. 11a). However, in the retention stage of cyclic peak stress, the rock bridge of sample M2 suddenly destroyed and three cracks were found close to the tip. During the second cyclic loading phase, the elastic modulus is reduced to 4.94 GPa. With the increase of axial stress, a tensile crack “C1” continue to expand slowly along the direction of maximum compressive stress (Fig. 11b). In the third cycle of cyclic loading phase, the elastic modulus decreases to 4.34 GPa, and the wing cracks length did not change significantly, but the width increased slightly as shown in Fig 11(b). The elastic modulus of the sample M1 at fourth (last) loading phase decreased to 4.28 GPa, and the crack propagation was not obvious in this loading stage. With the increase of axial stress, a tensile crack C1 continue to expand quickly along the direction of maximum compressive stress (Fig. 11c). In the fourth cycle of cyclic loading phase, the elastic modulus decreases to 3.16 GPa, the width

and length of wing cracks change significantly as shown in Fig 11(c). The failure process simulated by using origin software and laboratory test as shown in Fig. 11(d) were same showing the accuracy of current study. It could be seen that after the fourth cycle of loading and unloading phase, the connection between the structures of sample “M1” does not completely disappeared and the change of transverse deformation has been relatively stable. So, the sample did not break at this time. The transverse deformation of the sample was still stable at the initial stage of the sixth loading cycle, when the axial stress was about 15.5MPa. The first five weeks of loading and unloading cyclic phase lead to the propagation of cracks and weakening the bearing structure of the sample. Finally, it causes the sample to breakdown in advance during the loading phase of the six week of loading and unloading cycles. Since the stress value at the failure point is smaller than that of peak stress of the last loading week. the peak stress of the sample M1 is essentially the peak stress of the fifth cycle [14].

Observing the cyclic loading and unloading phases of all samples, the following rules can be found: except for the samples of group M1, the other groups of samples are mainly characterized by the elastic modulus “strengthening” phenomenon. The appearance of the sample in the third loading is still intact, and the elastic modulus also shows the “strengthening” phenomenon [14]. However, during the third week of cyclic peak stress retention, the sample N3 suddenly sprouted a plurality of cracks, and the bearing structure of the sample was weakened, which directly led to the “weakening” phenomenon of the elastic modulus,

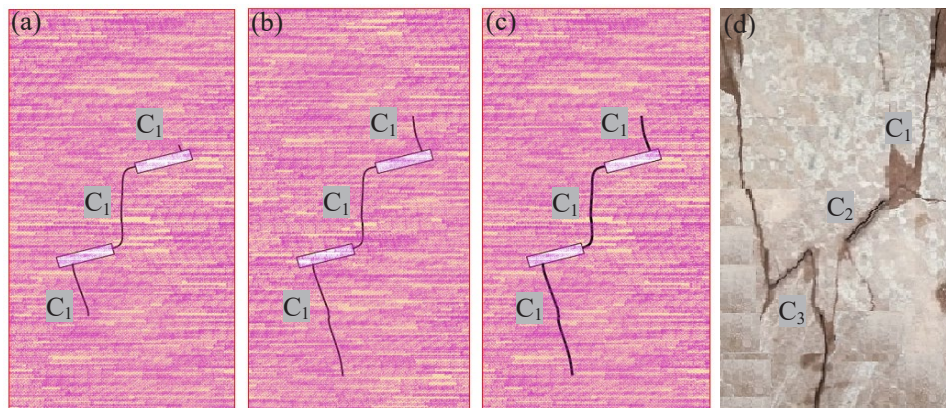


Fig. 11. Failure process diagram of samples (a) after second cycle (b) after third cycle (c) after fourth cycle (d) failure pattern diagram

this is also highlighted by Zhou et al. [17]. During the fourth cyclic loading phase the elastic modulus of the sample N2 begins to decrease gradually after that, and the gradual weakening of the elastic modulus is always accompanied by the propagation of macroscopic cracks and also, the relationship between them was quite close.

4. ANALYSIS OF DAMAGE EVOLUTION LAW

4.1 Damage Variable

In the laboratory tests, the damage variable is usually not directly detected on the surface of the specimen. Therefore, the definition of damage is the key to study the evolution law of rock material during loading. It is known from the basic principles of thermodynamics that the definition of different angles of damage is essentially equivalent and the damage variable is defined by the strain during the applied loading on the samples as:

$$D_i = \varepsilon_i^{\max} / \varepsilon_N^{\max}$$

Where; D_i is damage degree in the i (initial) cyclic stage, ε_i^{\max} is the maximum axial strain at initial cyclic stage, and ε_N^{\max} is the maximum axial strain at the last cyclic stage.

When $i = 0$, the sample is in an unloaded state, so the corresponding $\varepsilon_N^{\max} = 0$, and the damage degree is $D_0 = 0$. When the sample is in the loaded state but has not been destroyed, $\varepsilon_i^{\max} \neq 0$ and $\varepsilon_i^{\max} < \varepsilon_N^{\max}$, then the damage degree of the sample is $0 < D_i < 1$. When the sample is destroyed $\varepsilon_i^{\max} = \varepsilon_N^{\max}$, so $D_i = 1$, the damage degree of the sample reaches the peak.

4.2 Damage Evolution Equation of Specimen Under Cyclic Load

The damage energy release rate during the loading process can be obtained by using the following equation as:

$$Y_i = \frac{U_i^e}{1 - D_i}$$

Where U_i^e is the elastic energy, D_i is the damage variable, and Y_i is the dissipation energy. From the damage Eq. 4, it can be seen that the release rate of dissipated energy is the same as the dimension of

dissipated energy and elastic energy.

The damage variable and the elastic energy obtained by using the damage state Eq. 4. The damage evolution equation of rock during loading is as follows:

$$D_i = 1 - \exp\left[-B|Y_i - Y_0|^{\frac{1}{n}}\right]$$

Where D_i is damage variable at the stage i cycle and B , n , and Y_0 are rock material constants, depending on the material's own characteristics. Taking the logarithm of the two sides of the Eq. 5 the damage degree can be obtained as:

$$\ln[-\ln(1 - D_i)] = \frac{1}{n} \ln|Y_i - Y_0| + \ln B$$

Let $y = \ln[-\ln(1 - D_i)]$, $nx = \ln|Y_i - Y_0|$, $b = \ln B$, then the Eq. 6 can be further simplified into the following linear relations:

Where $k=1/n$, $b = \ln B$.

The degree of damage D_i and the dissipative energy release rate was analyzed by linear fitting analysis. The experimental and theoretical curve of the damage evolution of the sample in the fitted straight line can be further determined by using above equation system and plotted as Fig. 12. The theoretical damage evolution is in good agreement with the actual experimental data. This indicates that the damage evolution equation can reflect the damage evolution of prefabricated cracked sandstone during cyclic loading.

4.3 Damage Evolution Law

The damage evolution law of the samples of M and N group is shown in Figs. 12. The results from origin software are used to plot Fig. 12. Also, Fig. 12 shows the relationship between damage degree and strength degradation of sandstone specimens. Concave down relationship between damage degree and strength degradation is found in all fourth cases as shown in (Fig. 12a-d). When the damage degree was high, the damage evolution curve is obviously concave down (Fig. 12a-b). Fig. 12 (c-d) clearly shows that as damage degree decreases damage evaluation curve become linear.

In the damage-loading curve, the inflection point is a turning point of the damage evolution process (Fig. 13). Before this point, the main change of fitting curves occurs in the second and third peaks (see Fig. 13), which indicates that the micro damage of sandstone is caused by sharp

increase in size and number of micro cracks. Whereas, after this point, the fourth peak of the fitting curves increases rapidly as displayed in Fig. 13. This figure indicates that the cracks are increasing and the fatigue damage of sandstone is caused by prefabricated crack connection.

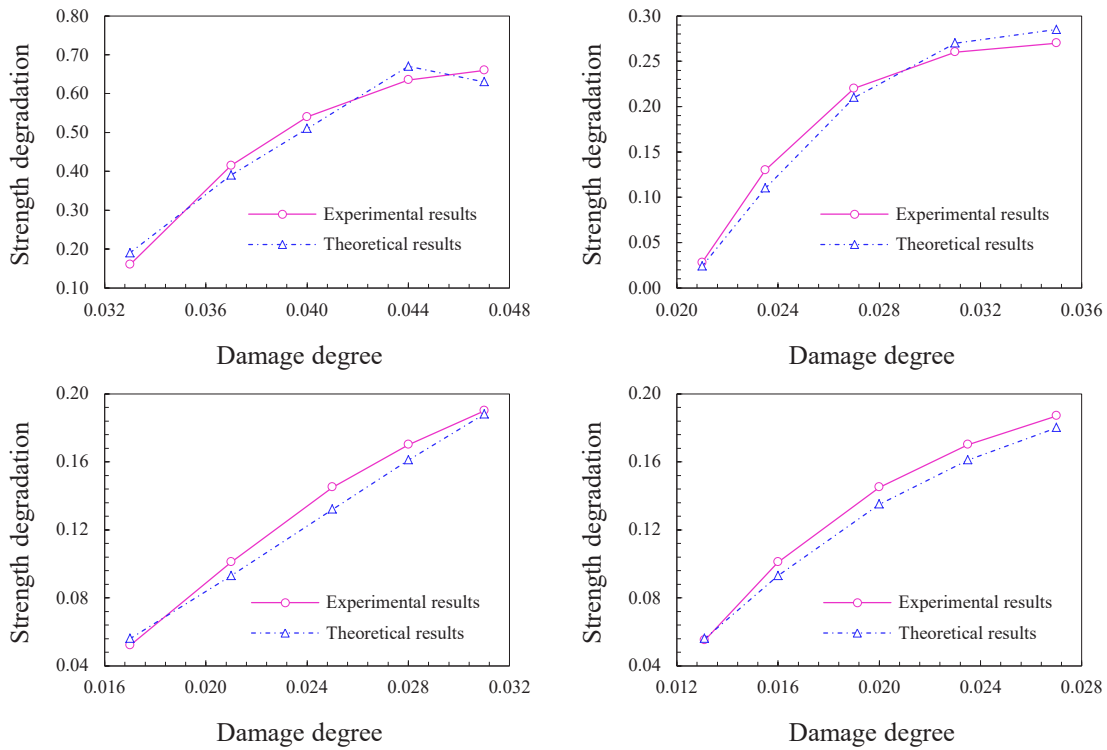


Fig. 12. Theoretical and experimental comparison curves of damage growth

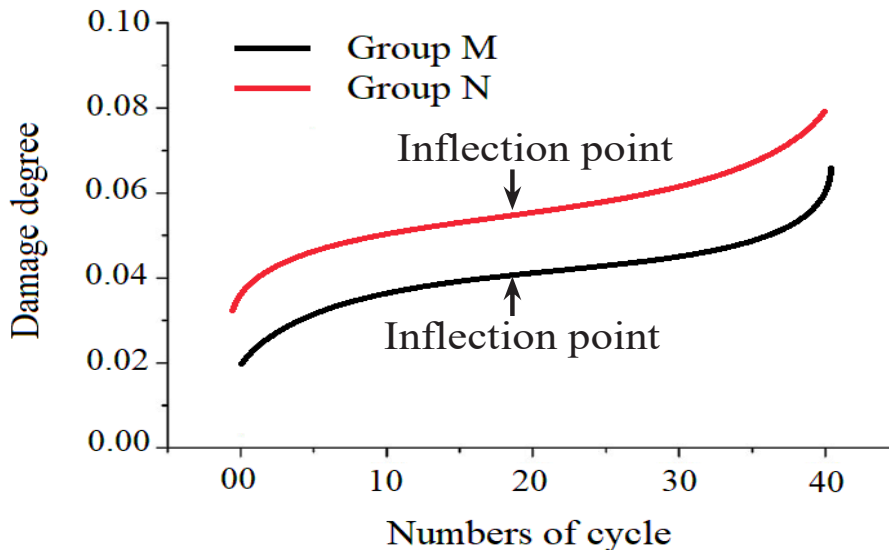


Fig. 13. damage degree vs the number of loading cycles

5. CONCLUSIONS

From the origin software and laboratory tests of sandstone samples performed at cyclic upper limit stress was 24.0, 26.0, 28.0, 30.0, 32.0 and 34.0 MPa, the following conclusions are drawn:

1. The change of macro-mechanical properties of rock under cyclic loading is basically for the external appearance in change of internal micro-structure of cracked sandstone samples. The difference in peak strengths of sandstone samples under cyclic loading is closely related to its cyclic stress level and compressive strength and compactness. Based on the meso-mechanism analysis sandstone samples showed “strengthening” phenomenon at peak strength.
2. The elastic modulus increases gradually after six weeks of loading and unloading cycles. With the increase of the number of loading cycles, the elastic modulus of prefabricated cracked sandstone specimens also presented a “strengthening” phenomenon.
3. Crack geometric parameters (α and β) significantly influence the stress eigenvalues of sandstone specimens. With the increase of α , the crack initiation stress and the peak strength of samples first increased and then decreased, while with the increase of β , the crack initiation stress and the peak strength first decreased and then increased. The variation of peak stress and crack initiation stress were very similar with crack geometric parameters, and the effect of α on stress eigenvalues were more significant compare to β . Also, the dip angle of rock bridge has a great effect on the coalescence mode of rock bridge. When β was 30°, 45° and 60° the crack bridge area showed composite coalescence and when β was 75° and 90° the crack bridge area showed tension coalescence.

6. REFERENCES

1. Y. Zong., L. Han., S. Wen., Y. Zong, and J. Wei. Experimental Study on Mechanical and Damage Evolution Properties of Sandstone under Triaxial Compression. 13th ISRM International Congress of Rock Mechanics, *International Society for Rock Mechanics and Rock Engineering*, 1-14: (2015).
2. E. Liu., S. He., X. Xue, and J. Xu. Dynamic properties of intact rock samples subjected to cyclic loading under confining pressure conditions. *Rocks Mechanics and Rocks Engineering*, 44(5): 629-634 (2011).
3. J. Xiao., D. Ding., G. Xu, and F. Jiang. Waveform effect on quasi-dynamic loading condition and the mechanical properties of brittle materials. *International Journal of Rock Mechanics and Mining Sciences*, 45(4) 621-626 (2008).
4. N. Li., W. Chen., P. Zhang, and G. Swoboda. The mechanical properties and a fatigue-damage model for jointed rock masses subjected to dynamic cyclical loading. *International Journal of Rock Mechanics and Mining Sciences*, 38(7): 1071-1079 (2001).
5. T. Zhenyu, and M. Haihong. An experimental study and analysis of the behaviour of rock under cyclic loading. *International Journal of Rock Mechanics and Mining Sciences*, 27(1): 51-56 (1990).
6. K. Fuenkajorn, and D. Phueakphum. Effects of cyclic loading on mechanical properties of Maha Sarakham salt. *Engineering Geology*, 112(1-4): 43-52 (2010).
7. Y. Tien., D. Lee, and C. Juang. Strain, pore pressure and fatigue characteristics of sandstone under various load conditions. *International Journal of Rock Mechanics and Mining Sciences & Geomechanics Abstracts, Elsevier*. 283-289 (1990).
8. A. Momeni., M. Karakus., G. Khanlari, and M. Heidari. Effects of cyclic loading on the mechanical properties of a granite. *International Journal of Rock Mechanics and Mining Sciences*, 100(77): 89-96 (2015).
9. H. Xie., Y. Ju, and L. Li. Criteria for strength and structural failure of rocks based on energy dissipation and energy release principles. *Chinese Journal of Rock Mechanics and Engineering*, 24(17): 3003-3010 (2005).
10. J. Xiao., D. Ding., G. Xu, and F. Jiang. Inverted S-shaped model for nonlinear fatigue damage of rock. *International journal of rock mechanics and mining sciences*, 46(3): 643-648 (2009).
11. L. Yun-De., G. Xiu-Run, and Y. Jiang. Study on conventional triaxial compression test of complete process for marble and its constitutive equation. *Chinese Journal of Rock Mechanics and Engineering*, 23(15): 2489-2493(2004).
12. J. Ren. Rock meso-damage propagation law in the triaxial compression loading and its constitutive model. *Journal of China Coal Society*, 26(6): 578-583 (2001).
13. P. Jin., E. Wang., X. Liu., N. Huang, and S. Wang. Damage evolution law of coal-rock under uniaxial compression based on the electromagnetic radiation

- characteristics. *International Journal of Mining Science and Technology*, 23(2): 213-219 (2013).
14. Z. Zhang., W. Xu., W. Wang, and R. Wang. Investigation on conventional triaxial compression tests of ductile rock and law of deformation and damage evolution. *Chinese Journal of Rock Mechanics and Engineering*, 30(S2): 3857-3862 (2011).
 15. X. Ni, and Z. Xj. Quantitative test study of meso-damage of granite under cyclic load with different frequencies. *Rock and Soil Mechanics*, 33(2): 422-427 (2012).
 16. S. Cattaneo, and J. Labuz. Damage of marble from cyclic loading, *Journal of Materials in Civil Engineering*, 13(6): 459-465 (2001).
 17. J. Zhou., X. Yang., W. Fu., J. Xu., H. Li., H. Zhou, and J. Liu. Experimental test and fracture damage mechanical characteristics of brittle rock under uniaxial cyclic loading and unloading conditions. *Chinese Journal of Rock Mechanics and Engineering* 29(6): 1172-1183 (2010).
 18. T. Wen., Wen., Y. Liu., K. Wang, and C. Yang. Modified statistical damage constitutive model of rock based on normal distribution. *Electronic Journal of Geotechnical Engineering*, 19(24): 16931-16947 (2014).
 19. X. Jiang., L. Shu-chun., T. Yun-qi., T. Xiao-jun, and W. Xin. Acoustic emission characteristic during rock fatigue damage and failure. *Procedia Earth and Planetary Science*, 1(1): 556-559 (2009).
 20. Y. Kang., Z. Zhang., H. Wang, and Q. Qin. Experimental investigations of the effect of thickness on fracture toughness of metallic foils. *Materials Science and Engineering*, 394(1-2): 312-319 (2005).
 21. B. Pan., K. Qian., H. Xie, and A. Asundi. Two-dimensional digital image correlation for in-plane displacement and strain measurement: a review. *Measurement Science and Technology*, 20(6): 062001 (2009).
 22. T. Nguyen., S. Hall., P. Vacher, and G. Viggiani. Fracture mechanisms in soft rock: identification and quantification of evolving displacement discontinuities by extended digital image correlation. *Tectonophysics*, 503(1-2): 117-128 (2011).
 23. H. Zhang., G. Huang., H. Song, and Y. Kang. Experimental investigation of deformation and failure mechanisms in rock under indentation by digital image correlation. *Engineering Fracture Mechanics*, 96: 667-675 (2012).
 24. H. Zhang., H. Song., Y. Kang., G. Huang, and C. Qu. Experimental analysis on deformation evolution and crack propagation of rock under cyclic indentation. *Rock Mechanics & Rock Engineering*, 46(5): 1053-1059 (2013).
 25. M. Sutton., J. Orteu, and H. Schreier. Image correlation for shape, motion and deformation measurements: basic concepts, theory and applications, Springer Science & Business Media (2009).
 26. A. Mudassar, and S. Butt. Improved digital image correlation method. *Optics and Lasers in Engineering*, 87:156-167 (2016).
 27. B. Pan., A. Asundi., H. Xie, and J. Gao. Digital image correlation using iterative least squares and pointwise least squares for displacement field and strain field measurements. *Optics and Lasers in Engineering*, 47(7-8): 865-874 (2009).
 28. J. Xiao., D. Ding., F. Jiang, and G. Xu. Fatigue damage variable and evolution of rock subjected to cyclic loading. *International Journal of Rock Mechanics & Mining Sciences*, 47:461468 (2010).
 29. C. Khazaei., J. Hazzard, and R. Chalaturnyk. Damage quantification of intact rocks using acoustic emission energies recorded during uniaxial compression test and discrete element modeling. *Computers and Geotechnics*, 67:94-102s(2015).

